



Influence of steaming on the acidity and the methanol conversion reaction of HZSM-5 zeolite



Sami M.T. Almutairi, Brahim Mezari, Evgeny A. Pidko, Pieter C.M.M. Magusin, Emiel J.M. Hensen*

Schuit Institute of Catalysis, Laboratory of Inorganic Materials Chemistry, Eindhoven University of Technology, Den Dolech 2, 5600 MB Eindhoven, The Netherlands

ARTICLE INFO

Article history:

Received 21 May 2013

Revised 16 July 2013

Accepted 21 July 2013

Keywords:

Zeolite
HZSM-5
Acidity
Steaming
Methanol

ABSTRACT

The influence of steaming at varying temperatures on the physicochemical properties of a HZSM-5 zeolite (Si/Al = 27) was investigated by X-ray diffraction, ^{27}Al MAS NMR, Ar physisorption and IR spectroscopy of adsorbed pyridine, 2,4,6-trimethylpyridine and CO. The catalytic activity of the zeolites was evaluated in propane and methanol conversion reactions. Mild steaming did not result in removal of framework Al atoms. Instead, evidence was found that some extra-framework Al atoms present in the parent zeolite were inserted into the framework at defect sites. This resulted in higher propane conversion rates. Severe steaming resulted in a strong decrease in the framework Al content and agglomeration of extra-framework Al atoms. This caused a strong decrease in the Brønsted acidity probed by pyridine and CO IR. The rate of propane conversion was consequently adversely affected. The steaming procedures did not result in the formation of noticeable mesoporosity. By IR spectroscopy of adsorbed 2,4,6-trimethylpyridine, however, indications were found for structural damage at the outer region of the zeolite crystals, resulting in increased accessibility of the Brønsted acid sites (BAS). For methanol conversion at 350 °C, the concentration of BAS governs the catalytic performance. For zeolites with a high BAS density (parent and mildly steamed zeolites), the rate of deactivation is high. The total amount of methanol converted per BAS is relatively low because of the high rate of consecutive reactions. These reactions involve the conversion of the dehydration product of methanol, dimethyl ether, to products with carbon-carbon bonds and the formation of carbonaceous deposits, which deactivate the zeolite catalyst. Decreasing Brønsted acidity by severe steaming results in an increased amount of methanol converted per BAS because of the lower coke formation rate. As a result, the total amount of methanol converted per BAS increases strongly with decreasing BAS density. However, it also causes lower rates of conversion of dimethyl ether to useful products. In terms of the total amount of methanol converted per BAS to light olefins, the set of zeolites shows optimum performance at intermediate BAS density (HZSM-5 severely steamed at 450 °C; concentration of BAS $\sim 0.2 \text{ mmol g}^{-1}$).

© 2013 Elsevier Inc. All rights reserved.

1. Introduction

Zeolites are crystalline microporous aluminosilicates, which are extensively used in industry to catalyze a wide variety of reactions. The acid catalytic activity of zeolite resides in tetrahedral framework Al atoms. The charge-compensating protons of the oxygen anions bridging between Al and Si give rise to strong Brønsted acidity [1]. Hydrolytic removal of Al atoms from their framework sites (dealumination) is an important method to modify the catalytic properties of zeolites. Dealumination by steam calcination is a key technology in the manufacture of strongly acidic and accessible faujasite-based cracking zeolites [2–5]. Besides conventional (steam) calcination [6,7], dealumination can also be done by post-synthesis modification such as treatment with SiCl_4 [8],

chelating agents like EDTA [9] and $(\text{NH}_4)_2\text{SiF}_6$ [10], or leaching with HCl [11–13]. Typically, the removal of Al from the framework results in lower density of Brønsted acid sites (BAS). The extra-framework Al atoms may have a positive influence on the intrinsic acidity of the zeolite [14–16].

Typically, high-silica zeolites such as HZSM-5 are more stable than low-silica ones such as faujasites, thus requiring more severe conditions to dealuminate them [17,18]. Enhanced cracking activity of mildly steamed ZSM-5 has been attributed to the presence of extra-framework Al (EFAl) [14,19,20]. The nature of such EFAl atoms and the way they affect acid activity is not completely understood. Several types of octahedral Al atoms have been identified by ^{27}Al MAS NMR spectroscopy [21]. In addition, tetrahedral Al atoms may be present at ion-exchange positions and they may be invisible in NMR spectra due to strong quadrupolar broadening [22]. Neutral species such as monomeric AlOOH , $\text{Al}(\text{OH})_3$ [23], aluminum-oxo and hydroxo clusters [24–27], and bulk aluminum

* Corresponding author.

E-mail address: ej.m.hensen@tue.nl (E.J.M. Hensen).

oxide aggregates have also been reported for dealuminated zeolites [28,29]. The extraction of framework Al may also affect the pore structure and porosity by generation of voids larger than the original micropores. In addition, pores may become blocked by aggregated forms of Al. Usually, the number of Brønsted acid sites in HZSM-5 decreases with increasing dealumination time [30]. Lercher and co-workers showed that at relatively low steaming temperature (450 °C), isolated Al atoms are more prone to extraction from the lattice than Al atoms in close proximity to other Al-occupied tetrahedra [31]. In some cases, enhancement of protolytic *n*-alkane cracking has been reported upon mild steaming of HZSM-5 [14,32], which has been ascribed to synergy between Brønsted and Lewis acid sites [14]. Besides changes in the number and strength of the BAS, also their location is of crucial importance to the final catalytic performance. Dealumination can also result in surface roughening of the zeolites crystals and mesoporosity [33]. Mild steaming results in mesoporosity at the perimeter of the zeolite crystals, whereas steaming at 700 °C results in uniformly distributed mesopores. Severe dealumination of HZSM-5 suppresses coke formation and increases the performance during methanol conversion reactions [34]. The formation of carbonaceous residue in the course of the catalytic reaction deactivates the internal BAS. For methanol conversion, it is advantageous to have a low density of BAS because it lowers the rate of coke formation [35,36].

Herein, we investigate the influence of steaming on the acidic properties of HZSM-5 zeolite and the methanol conversion reaction. For this purpose, the steam flow and steam temperature were varied. The parent and modified ZSM-5 zeolites were characterized by XRD, Ar physisorption, ²⁷Al MAS NMR spectroscopy and FTIR spectroscopy of pyridine, 2,4,6-trimethylpyridine, and CO. The catalytic activities of these zeolites are compared in propane and methanol conversion.

2. Experimental procedures

2.1. Synthesis of materials

The parent NH₄ form of ZSM-5 (SM-55) zeolite (SAR = 55) was obtained from Süd-Chemie. The proton form of the zeolite was obtained by calcination in a mixture of 20 vol.% oxygen in nitrogen at a flow rate of 100 Nml/min, while heating to 550 °C at a rate of 5 °C/min followed by an isothermal period of 6 h. This parent zeolite was further treated by mild and severe steaming with 100% water vapor. A first set was prepared by heating zeolite (in 1 g batches) to the steaming temperature under He flow, followed by steaming at a total flow rate of 8.2×10^{-5} mol min⁻¹ at 400, 450, 500, 550, and 600 °C for 6 h. These zeolites are denoted by HZSM-5(*ms*, *x*) with *ms* referring to mild steaming and *x* to the final steaming temperature in °C. For severe steaming, a higher steam flow rate of 3.3×10^{-4} mol min⁻¹ was employed under otherwise similar conditions. These zeolites are denoted by HZSM-5(*ss*, *x*). The steaming treatments were performed in a fixed-bed calcination oven (shallow bed).

2.2. Catalyst characterization

2.2.1. X-ray diffraction (XRD)

The integrity of the zeolite structure was characterized by X-ray diffraction (XRD). XRD patterns were recorded on a Bruker D4 Endeavor Diffractometer using Cu K α radiation with a wavelength of 1.54056 Å. 2 θ angles from 5° to 60° were measured with a step size of 0.077° and a time per step of 1 s. The catalysts were ground and pressed in sample holders for measurements. The Topas software

(Bruker) was used to calculate the crystallinities of the zeolite samples from the XRD patterns.

2.2.2. Ar physisorption measurements

Ar sorption measurements were performed at -186 °C on a Micromeritics ASAP-2020 apparatus in static measurement mode. In a typical experiment, a zeolite sample (~100 mg) was outgassed at 350 °C for 8 h prior to the sorption measurement. The Brunauer–Emmett–Teller (BET) equation was used to calculate the specific surface area from the adsorption data obtained in the *p/p*₀ range of 0.05–0.25. The volume of mesopores (*V*_{meso}) and the area of mesopores (*S*_{meso}) were calculated using the Barrett–Joyner–Halenda (BJH) method on the adsorption branch of the isotherm. The micropore area (*S*_{micr}) and micropore volume (*V*_{micr}) were calculated, employing the *t*-plot method using the thickness range between 3.4 and 5.0 Å.

2.2.3. Thermogravimetric analysis (TGA)

TGA measurements were performed on Mettler TGA/DSC-1 connected to gas analysis system (ThermoStar™) using the following conditions: 70 μ l alumina crucibles, dry air as a purge gas, and nitrogen as a protective gas with flows of 40 ml min⁻¹ each. In a typical experiment, the temperature was increased from 40 to 850 °C at a rate of 5 °C min⁻¹.

2.2.4. ²⁷Al MAS NMR spectroscopy

Magic angle spinning (MAS) ²⁷Al single pulse NMR spectra were recorded on a Bruker DMX500 NMR spectrometer operating at a magnetic field of 11.7 T. The ²⁷Al NMR frequency was 130 MHz. The ²⁷Al chemical shift is referred to a saturated Al (NO₃)₃ solution. In a typical experiment, about 10 mg of well-hydrated sample was accurately weighed and packed in a 2.5-mm zirconia rotor. The sample rotation speed was 20 kHz. Single-pulse excitation was used with a 20° pulse of 1 μ s and a relaxation delay of 1 s, which allowed quantitative measurements as judged from test spectra with longer pulse duration (2 μ s) or relaxation delay (2 s). Prior to NMR measurements, the samples were hydrated in a desiccator. NMR spectra were also recorded after treating the mildly dried zeolite in a flow of ammonia (10% NH₃ in He) at 120 °C. These samples are denoted by the use of the suffix -NH₃.

2.2.5. Infrared spectroscopy of adsorbed pyridine, 2,4,6-trimethylpyridine, and CO

Brønsted and Lewis acidity of the zeolites was investigated by FTIR spectroscopy of adsorbed pyridine and 2,4,6-collidine (2,4,6-trimethylpyridine). FTIR spectra were recorded in a Bruker Vertex V70v FTIR spectrometer in transmission mode. In a typical experiment, a zeolite sample was pressed into a self-supporting wafer with a density of 5–6 mg cm⁻². The wafer was placed in a controlled-environment transmission cell equipped with CaF₂ windows. Prior to recording the spectra, the zeolite was dehydrated in an oxygen flow under heating from ambient temperature to 550 °C at a rate of 5 °C min⁻¹. The sample was then evacuated at 550 °C for 0.5 h and cooled to 150 °C temperature in vacuum. During this pretreatment, the cell body and the evacuated gas-supply section of the setup were kept at 80 °C to remove remaining physisorbed water. The final pressure of the cell was lower than 2×10^{-6} mbar. The zeolite wafer was then exposed to pyridine at 150 °C. After a hold time of 20 min, the sample was evacuated for 1 h to remove physisorbed adsorbate and a first spectrum was recorded. Subsequently, the sample was heated to 350 °C, kept for 1 h at this temperature, and cooled to 150 °C. Then, a second spectrum was recorded. Finally, the sample was heated to 500 °C, kept for 1 h at this temperature, and cooled to 150 °C. Then, a third spectrum was recorded. Total Brønsted and Lewis acidity and the concentrations of weak, medium, and strong forms of these sites

were derived from these data. The concentrations were calculated on the basis of the molar extinction coefficient given by Datka et al. of 0.73 and 1.11 cm μmol^{-1} for BAS and LAS, respectively [37]. For some samples, additional IR experiments with 2,4,6-collidine were carried out in a similar fashion as done for pyridine. In this case, the strong Brønsted acid sites are reported on the basis of the intensity of the 1636 cm^{-1} band after evacuation at 500 °C. The extinction coefficient of 10.1 cm μmol^{-1} reported by Nesterenko et al. [38] was used.

For FTIR spectroscopy of adsorbed CO, the dehydrated catalyst wafer was cooled by flowing liquid nitrogen through a capillary spiraled around the catalyst wafer. After reaching liquid N₂ temperature, an initial spectrum was recorded. CO (Praxair, 99.999%) was dosed through a sample loop connected to a 6-way valve, allowing dosing accurate amounts of CO (0.04 mmol) to the cell in a computer-controlled sequence. Difference spectra were obtained by subtracting the initial spectrum of the dehydrated catalyst from the spectra obtained at increasing CO coverage. Spectra were normalized to the catalyst wafer weight.

2.2.6. Propane cracking

The acid activity of the zeolites was determined by measuring the rate of monomolecular cracking of propane. Catalytic activity measurements were performed in an atmospheric-pressure single-pass quartz microflow reactor at 550 °C. The feed mixture was delivered by thermal mass flow controllers and consisted of 5 vol.% C₃H₈ in He at a total flow rate of 100 ml/min. The WHSV space velocity was kept at 11.7 h⁻¹. The product composition was analyzed by an online three-column gas chromatograph (Compact GC Interscience) equipped with a PLOT Al₂O₃/KCl column with a flame ionization detector and Molsieve-5 Å and RTX-1 columns both employing thermal conductivity detectors. The conversion was kept below 5% to ensure differential conditions. The reaction rates (r) were calculated by use of $r = X \cdot \frac{F}{m_{\text{cat}}}$, where X is conversion of propane, F is flow rate in mol s⁻¹, and m_{cat} is the weight of the catalyst in g.

2.2.7. Methanol conversion

The catalytic activity in the methanol to olefins reaction was determined in a quartz tubular fixed-bed reactor. The catalyst was placed as pressed, crushed, and sieved particles in the 125–250 μm range between two quartz wool plugs. Prior to reaction, the catalyst was activated at 550 °C in artificial air (30 ml min⁻¹) for 2 h. The methanol conversion was performed at 350 °C. Methanol (Merck, 99%) was introduced to the reactor by flowing He through a saturator containing the reactant. The WHSV was kept at 6.65 g_{MeOH} g_{cat}⁻¹ h⁻¹, and the effluent was analyzed by online gas chromatography (Compact GC, Interscience) equipped with TCD and FID detectors with RT-Q-Bond and Al₂O₃/KCl columns, respectively.

3. Results

3.1. Structural characterization

The XRD patterns (see Supporting information, Fig. S1) show that the structure of HZSM-5 is not significantly affected by the steaming treatment. All zeolites retain the MFI topology and their initial high crystallinity (Table S1). The lattice parameters and the unit cell volumes do not vary significantly for the mildly steamed HZSM-5 samples. Steaming under severe conditions shows a more substantial contraction of the lattice parameters and unit cell volume, especially at higher steaming temperatures. These changes point to the removal of Al from the zeolite framework.

The textural properties of the parent and treated ZSM-5 zeolites are given in Table 1. The BET surface areas of the steamed zeolites are lower than those of the parent material. Typically, the micropore volume and surface area decreased because of the steaming treatment. However, there is no clear trend with the severity of the treatment, except that severe steaming at elevated temperatures leads to a slightly stronger decrease in the surface area. The textural properties do not evidence the formation of significant mesoporosity in the treated zeolites.

²⁷Al MAS NMR spectra for the parent (HZSM-5) and steamed zeolites are shown in Fig. 1. The spectra clearly show that the main effect of the steaming treatment is partial extraction of framework Al atoms to extra-framework positions. The spectrum of the parent HZSM-5 zeolite contains a strong signal around 55 ppm corresponding to tetrahedral framework Al atoms and a weak one around 0 ppm corresponding to extra-framework Al atoms in octahedral coordination. The intensity of the peak around 55 ppm decreased slightly with steaming temperature for the mildly steamed zeolites. The loss of framework Al was not quantitatively compensated by an increase in the signal of extra-framework species (cf. Al^{visible} in Table 2), implying that NMR-invisible Al nuclei are formed. The dealumination degree did not appreciably change anymore when the steaming treatment was done at temperatures above 500 °C. The results are different when steaming is carried out under severe conditions. The intensity of the signal due to tetrahedral Al decreased progressively with increasing steaming temperature. A broad peak at 30 ppm appeared in the NMR spectra, which is assigned to framework Al atoms in a distorted tetrahedral coordination or penta-coordinated Al atoms.

Treatment in NH₃ led to complete disappearance of Al^{VI} in the spectra of HZSM-5(ms, 500), HZSM-5(ms, 550) and HZSM-5(ms, 600) (Fig. 2), evidencing that the octahedral Al atoms in these samples are still closely associated with the zeolite framework [39,40]. In contrast, the spectra of ammonia-treated severely steamed zeolites showed much less changes in the Al coordination, indicating that in this case, the Al atoms were dislodged from the framework and are part of a separate aluminum-rich phase. These qualitative trends are confirmed by the data reported in Table 2 obtained by

Table 1
Textural properties of ZSM-5 and steamed ZSM-5 zeolites as determined by Ar physisorption.

Sample	S_{BET} (m ² g ⁻¹)	S_{meso} (m ² g ⁻¹)	BJH_{meso} (m ² g ⁻¹)	V_{meso} (cm ³ g ⁻¹)	S_{micro} (m ² g ⁻¹)	V_{micro} (cm ³ g ⁻¹)
HZSM-5	326	37	19	0.033	288	0.14
HZSM-5(ms, 400)	267	31	13	0.026	236	0.11
HZSM-5(ms, 450)	270	34	15	0.027	236	0.11
HZSM-5(ms, 500)	n.d.	n.d.	n.d.	n.d.	n.d.	n.d.
HZSM-5(ms, 550)	270	26	12	0.023	244	0.12
HZSM-5(ms, 600)	291	31	12	0.025	260	0.12
HZSM-5(ss, 400)	291	38	16	0.031	253	0.12
HZSM-5(ss, 450)	291	39	17	0.034	253	0.12
HZSM-5(ss, 500)	293	39	17	0.036	254	0.12
HZSM-5(ss, 550)	257	32	14	0.028	225	0.11
HZSM-5(ss, 600)	238	27	13	0.026	210	0.1

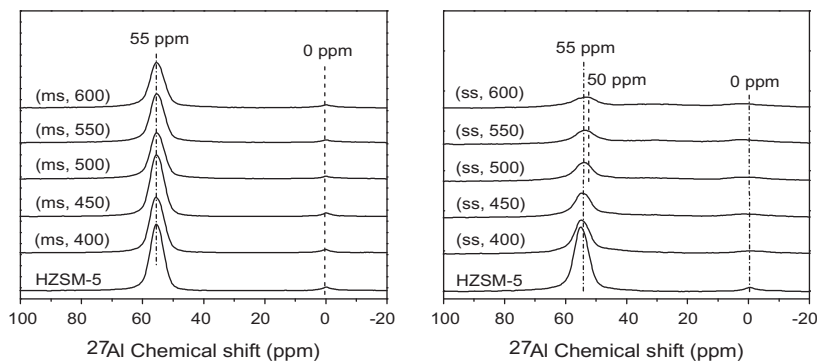


Fig. 1. ^{27}Al MAS NMR spectra of HZSM-5 treated under mild (left) and severe (right) steaming conditions.

Table 2

Al distribution and relative amount of Al species in the HZSM-5 and steamed ZSM-5 as determined by ^{27}Al NMR spectroscopy.

Sample	Al^{IV} (%)	$\text{Al}^{\text{distorted}}$ (%)	Al^{VI} (%)	$\text{Al}^{\text{visible}}$ (%)
HZSM-5	93	0	7	100
HZSM-5-NH ₃	100	0	0	100
HZSM-5(ms, 400)	92	0	8	90
HZSM-5(ms, 450)	91	0	9	95
HZSM-5(ms, 500)	90	0	10	86
HZSM-5(ms, 500)-NH ₃	100	0	0	89
HZSM-5(ms, 550)	93	0	7	88
HZSM-5(ms, 550)-NH ₃	99	0	1	90
HZSM-5(ms, 600)	90	0	10	85
HZSM-5(ms, 600)-NH ₃	100	0	0	88
HZSM-5(ss, 400)	67	17	16	65
HZSM-5(ss, 450)	56	24	20	60
HZSM-5(ss, 500)	47	28	24	59
HZSM-5(ss, 500)-NH ₃	68	23	9	77
HZSM-5(ss, 550)	40	30	30	57
HZSM-5(ss, 550)-NH ₃	54	16	30	69
HZSM-5(ss, 600)	40	30	30	56
HZSM-5(ss, 600)-NH ₃	37	35	26	61

deconvolution of the single pulse NMR spectra. The parent and the mildly steamed HZSM-5 zeolites all contain about 10% octahedral Al. All these species show flexible Al coordination. A small increase in the amount of NMR-invisible Al is noted with increasing steaming temperature. The severely steamed zeolites, however, contain a more significant fraction of octahedral and distorted tetrahedral/five-coordinated Al atoms. Their fraction strongly increases with the steaming temperature. Upon ammonia treatment, only some non-tetrahedral Al atoms revert their coordination to tetrahedral, indicating segregation of Al from the framework to a separate phase. This segregation of Al atoms becomes more significant with increasing steaming temperature.

3.2. Acidity characterization

The concentration and strength of the Brønsted acid sites and Lewis acid sites (LAS) was determined by IR spectroscopy of adsorbed pyridine. The acidic properties of the parent and steamed HZSM-5 zeolites are summarized in Table 3. The total BAS concentration for the parent zeolite is about 530 $\mu\text{mol/g}$. After evacuation at 300 °C, most of these sites are still covered with pyridine ($\sim 500 \mu\text{mol/g}$). The amount of LAS is in the range 70–110 $\mu\text{mol/g}$. Accordingly, the total acidity is close to 550–600 $\mu\text{mol/g}$ in reasonable agreement with the total Al content of the parent HZSM-5 zeolite. Care should be taken with the values determined by pyridine IR, as there is a large spread in reported values for the extinction coefficients for the pyridine ring vibrations representing BA and LA sites [41]. For mildly steamed zeolites, a maximum in the

concentration of BAS is observed after steaming at 550 °C. The increase in the BAS concentration goes together with a small decrease in the concentration of LAS. This may indicate that the steaming procedure causes reinsertion of extra-framework Al species into the framework or relocation/redispersion of such species to positions where addition of a nitrogen-containing base leads to reinsertion. Severe steaming results in considerable decrease in the total acidity. The higher the steaming temperature, the stronger the decrease in acidity. This is consistent with the trend in framework Al content determined by ^{27}Al NMR.

The presence of BAS at the external zeolite surface of the parent zeolite and of a subset of the steamed zeolites was probed by IR spectroscopy of adsorbed 2,4,6-collidine. In this case, only a single IR band around 1635 cm^{-1} due to protonated 2,4,6-collidine was observed. The concentrations of external BAS are given in Table 3. The data show an increasing amount of BAS accessible to 2,4,6-collidine with the severity of the steaming treatment. This trend is at odds with the one determined by pyridine IR. A tentative explanation is that framework damage close to the pore openings because of the steam treatment causes a slightly better accessibility of BAS close to the external surface.

The presence and strength of BAS and LAS in zeolite were also determined by IR spectroscopy of adsorbed CO (Fig. 3). At low temperature, the weak base CO can polarize the bridging hydroxyl groups. The strength of the BAS can be determined by measuring the stretching vibrations of the perturbed carbonyl, $\nu(\text{CO})$, and of the perturbed hydroxyl groups, $\nu(\text{OH})$. The interaction between the proton and CO results in a red shift of $\nu(\text{OH})$ and a blue shift of $\nu(\text{CO})$. The stronger these shifts, the stronger the Brønsted acidity of the hydroxyl group. The difference IR spectra of (steamed) HZSM-5 after CO adsorption are shown in Fig. 3. The most intense feature in the CO stretching region of HZSM-5 is observed at 2174 cm^{-1} , which is ascribed to CO adsorbed on strong BAS. The formation of CO condensed in the zeolite micropores results in a broad band with a maximum at 2138 cm^{-1} . In the hydroxyl-stretching region, two negative bands are observed at 3668 and 3616 cm^{-1} , which are respectively assigned to extra-framework Al hydroxide (Al–OH) and bridging hydroxyl (Si–OH–Al) groups. At these CO coverages, the non-acidic silanol groups are hardly perturbed. The OH stretching band is shifted to 3303 cm^{-1} , which corresponds to strong BAS. The spectra of the mildly steamed zeolites are qualitatively similar to those of the parent zeolite. The OH shift upon CO perturbation is very similar, indicating that the acid strength has not been changed due to mild steaming. A difference noted in the CO IR spectra of HZSM-5, HZSM-5(ms, 550), and HZSM-5(ms, 600) is the higher intensity of the bands related to the bridging hydroxyl groups for the latter two zeolites. This difference is consistent with the increase in BAS probed by pyridine IR. The spectra for the severely steamed zeolites (Figs. 3d and e) exhibit differences that are more distinct. Firstly, the spectra contain an

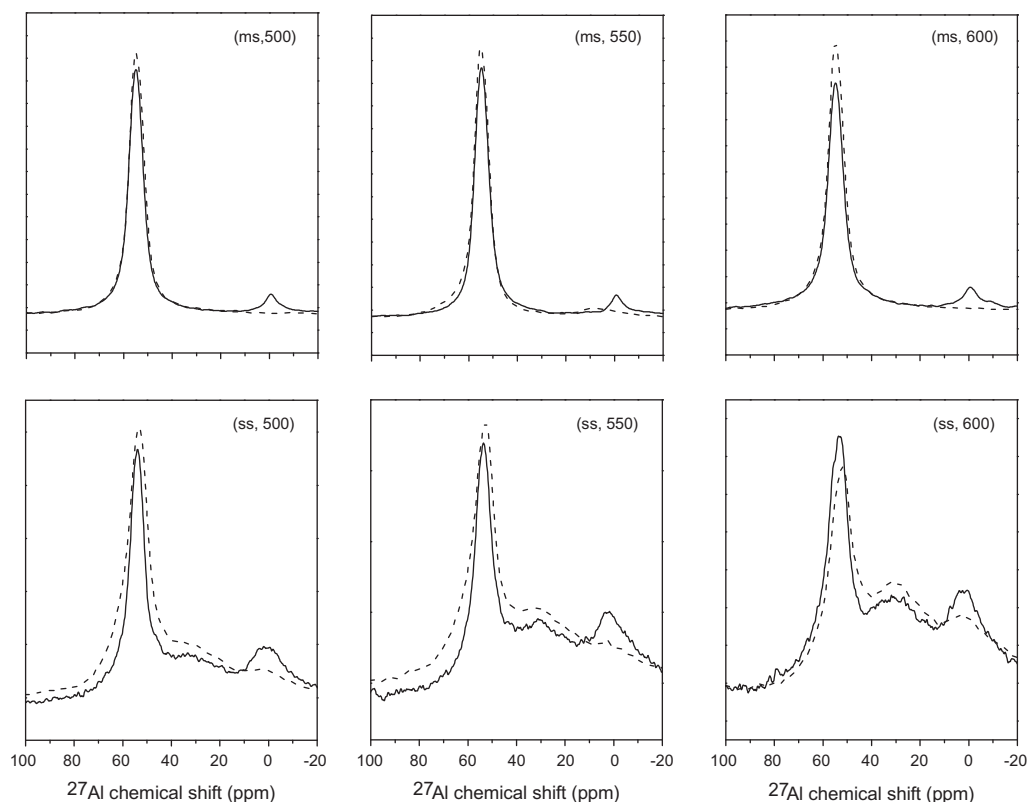


Fig. 2. ^{27}Al MAS NMR spectra before (full lines) and after (dashed lines) ammonia exposure of a selection of steamed ZSM-5 zeolites.

Table 3

Concentration of Brønsted and Lewis acid sites (IR spectroscopy of adsorbed pyridine) and external Brønsted acid sites (IR spectroscopy of adsorbed 2,4,6-collidine).

Sample	BAS ($\mu\text{mol/g}$) ^a	LAS ($\mu\text{mol/g}$) ^a	External BAS ($\mu\text{mol/g}$) ^a
HZSM-5	530	111	18
HZSM-5(ms, 400)	533	116	21
HZSM-5(ms, 450)	540	117	n.d. ^b
HZSM-5(ms, 500)	652	92	n.d.
HZSM-5(ms, 550)	814	90	23
HZSM-5(ms, 600)	668	88	n.d.
HZSM-5(ss, 400)	393	111	27
HZSM-5(ss, 450)	237	84	n.d.
HZSM-5(ss, 500)	130	51	n.d.
HZSM-5(ss, 550)	128	75	29
HZSM-5(ss, 600)	126	62	n.d.

^a Determined after evacuation at 150 °C.

^b Not determined.

additional band at 2168 cm^{-1} , which becomes more dominant at higher steaming temperature. This band is due to extra-framework AlOH–CO interactions [42]. In the hydroxyl region, a perturbed OH band in the region $3450\text{--}3500\text{ cm}^{-1}$ appears due to weaker BAS, likely related to extra-framework AlOH groups. Note that in the spectra of the parent and mildly steamed zeolites such bands are also present in the form of very weak shoulders. Secondly, a small number of weak Lewis acid sites are noticeable as follows from the appearance of a shoulder around 2190 cm^{-1} . Importantly, the red shift of $\nu(\text{OH})$ upon CO perturbation is similar for all zeolites, implying that the intrinsic acidity of the BAS in the various zeolites is similar. The CO_{ads} IR spectra do not evidence the presence of large amounts of Lewis acid sites. This may be taken as an indication that the dispersion of the extra-framework Al phase is relatively low.

Monomolecular cracking of propane at 550 °C was used as a test reaction to evaluate the acid catalytic activity of the zeolites. The conversion was kept below 5% in all cases. Accordingly, hydride transfer and secondary reactions are not expected to contribute to the catalytic performance. This is confirmed by the finding that the molar ratio of product ethylene and methane is close to unity for all zeolites. After the reaction, the catalyst was white, indicating that no significant amounts of coke deposits were formed. Table 4 collects the activity results, the overall reaction rate, the rates of propane cracking, and propane dehydrogenation. For propane cracking, the products are methane and ethylene. Propylene is the hydrocarbon product used to calculate the rate of propane dehydrogenation. The activities of the steamed HZSM-5 zeolites were different from the parent zeolite. Firstly, it is noted that among the mildly steamed zeolites, the highest activity is observed for HZSM-5(ms, 550). For this zeolite, both the overall conversion rate and the cracking and dehydrogenation activities are significantly higher than that of the parent zeolite. The activities of the zeolites steamed at lower temperatures are comparable to the reference, except for HZSM-5(ms, 400) with a much lower activity. The reason for this remains unclear especially in view of the results of pyridine IR, indicating that Brønsted acidity of this sample was unaltered. All of the severely steamed zeolites are less active in propane conversion than the parent zeolite. With increasing steaming temperature, the propane conversion and the rates of cracking and dehydrogenation strongly decrease in line with the spectroscopic results showing dislodging of Al from the framework and loss of strong Brønsted acid sites.

3.3. Catalytic activity measurements

Fig. 4 shows the activities of the parent and steamed zeolites in the methanol conversion reaction as a function of the time on

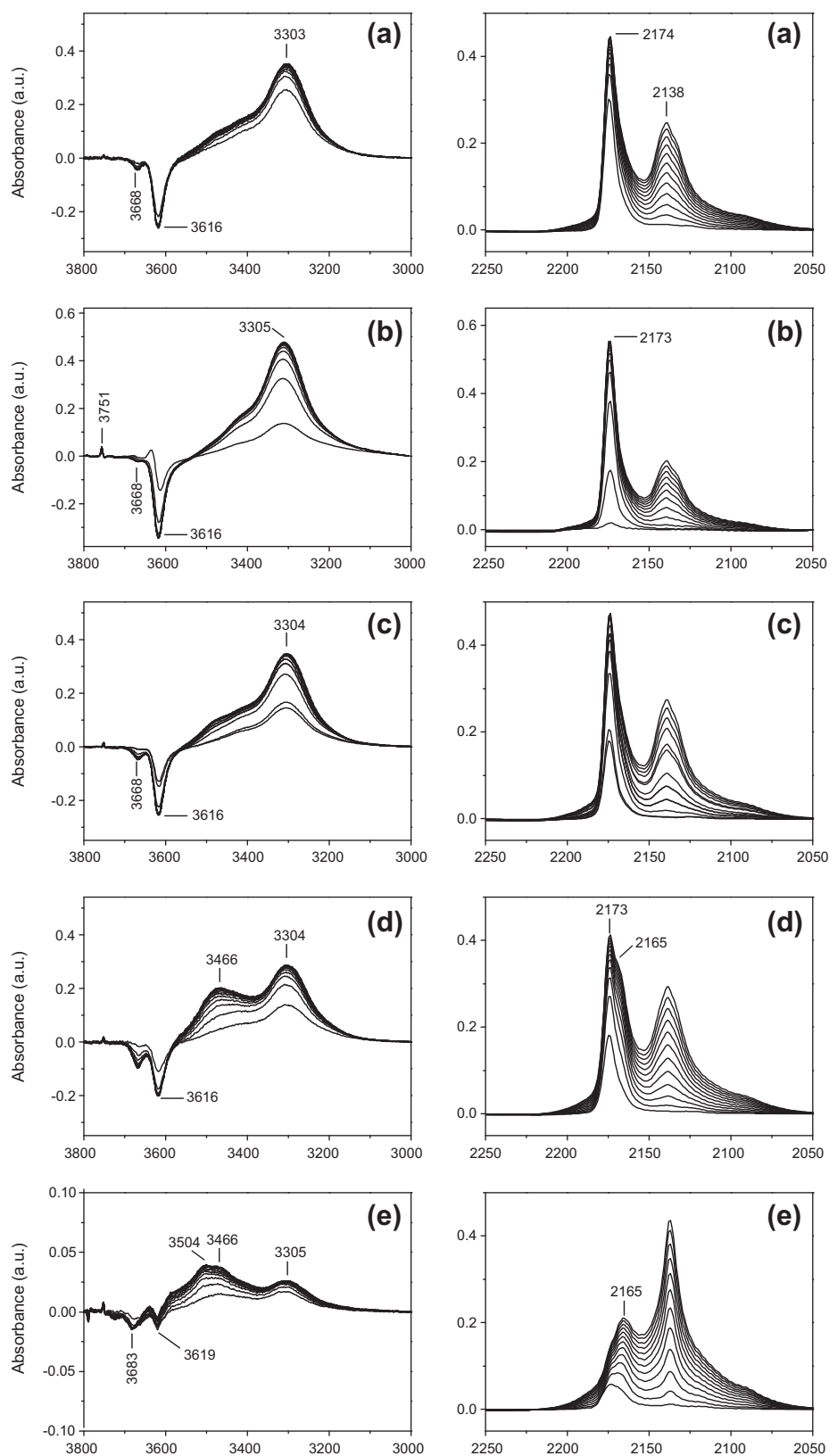


Fig. 3. Infrared spectra of the hydroxyl (left) and CO (right) stretching regions upon progressive adsorption of CO at 80 K for (a) HZSM-5, (b) HZSM-5(ms, 550), (c) HZSM-5(ms, 600), (d) HZSM-5(ss, 400), and (e) HZSM-5(ss, 600).

stream. The conversions and carbon selectivities are summarized in Table 5. For determination of the methanol conversion and selectivities, dimethyl ether was considered to be reactant. The

mildly steamed catalysts showed almost similar performance in the methanol conversion reaction as the parent zeolite. After 1 h, the methanol conversion for all these samples is close to 100%.

Table 4
Catalytic conversion of propane over hydrogen forms of ZSM-5 zeolites (WHSV = 11.7 h⁻¹; T = 550 °C).

Sample	$r^{\text{overall}} \times 10^{-5}$ (mol g ⁻¹ s ⁻¹)	$r^{\text{CRC}} \times 10^{-5}$ (mol g ⁻¹ s ⁻¹)	$r^{\text{deh}} \times 10^{-5}$ (mol g ⁻¹ s ⁻¹)	$r^{\text{deh}}/r^{\text{CRC}}$ ratio
HZSM-5	23.6	20.4	3.19	0.16
HZSM-5(ms, 400)	14.1	12.4	1.76	0.14
HZSM-5(ms, 450)	20.2	17.7	2.52	0.14
HZSM-5(ms, 500)	25.3	21.8	3.41	0.16
HZSM-5(ms, 550)	32.3	28.0	4.17	0.15
HZSM-5(ms, 600)	27.2	23.4	3.80	0.16
HZSM-5(ss, 400)	21.4	17.5	3.88	0.22
HZSM-5(ss, 450)	16.6	14.5	2.05	0.14
HZSM-5(ss, 500)	14.9	13.0	1.90	0.15
HZSM-5(ss, 550)	8.72	7.49	1.24	0.17
HZSM-5(ss, 600)	6.94	5.88	1.07	0.18

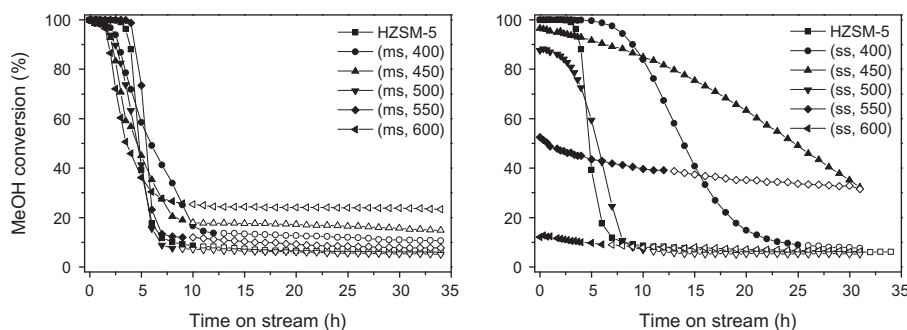


Fig. 4. Methanol conversion over the parent HZSM-5 zeolite and HZSM-5 after mild (left) and severe (right) steaming (WHSV = 6.65 g_{MeOH} g_{cat}⁻¹ h⁻¹; T = 350 °C). The open symbols indicate the regime where the rate of deactivation is smaller than 0.5%/h.

The propylene selectivity is slightly higher than the ethylene selectivity. Other products are higher hydrocarbons including some aromatics. The combined ethylene and propylene selectivity is around 60–65% for the mildly steamed samples and increases up to nearly 90% for the less acidic severely steamed ones. In addition, a substantial amount of propane is produced. After an initial period of complete methanol conversion (except for several weakly acidic zeolites), the methanol conversion decreases for all zeolites. Initially, the reactor effluent did not contain methanol and dimethyl ether, implying their complete conversion to products with carbon–carbon bonds. Thereafter, methanol was first observed in the reaction mixture and only at a somewhat later stage dimethylether. The concentration of methanol in the reactor effluent increased much faster with time on stream than the concentration of dimethylether. This suggests that methanol is directly converted into products with carbon–carbon bonds. Typically, only when the

methanol conversion had significantly decreased, equilibrium was established between methanol and dimethylether. For the least acidic zeolite HZSM-5(ss, 600), equilibrium between methanol and dimethylether was established already at the start of the catalytic experiment. For all catalysts, it is observed that a regime of strong catalyst deactivation is followed by residual activity in methanol conversion (indicated with open markers in Fig. 4). The low activity regime is characterized by a low rate of deactivation, which increased selectivity to lighter products at the expense of higher hydrocarbons. It is likely that the active sites for methanol conversion in this case are located at the outer region or the external surface of the zeolite crystals because carbonaceous deposits have blocked their micropore space.

The catalytic performance is expressed as a turnover number (TON) defined as the total amount of methanol converted into products with carbon–carbon bonds (products different from

Table 5
Methanol conversion and product selectivities after 1 h time on stream (WHSV = 6.65 g_{MeOH} g_{cat}⁻¹ h⁻¹; T = 350 °C; dimethyl ether not included in selectivities).

Sample	X_{MeOH} (%)	TON ^a	Coke (g/g) ^b	Selectivity(%)						
				CH ₄	C ₂ ⁼	C ₂	C ₃ ⁼	C ₃	C ₄	C ₅₊
HZSM-5	100	1.6×10^3	0.11	2.5	26	0.4	38	9	4	20
HZSM-5(ms, 400)	98	1.7×10^3	n.d.	0.8	22	0.2	42	8	8	19
HZSM-5(ms, 450)	98	1.5×10^3	n.d.	1.6	25	0.3	40	10	3	20
HZSM-5(ms, 500)	99	1.3×10^3	n.d.	1.6	25	0.3	37	11	3	22
HZSM-5(ms, 550)	100	1.2×10^3	n.d.	0.0	26	0.4	39	10	3	22
HZSM-5(ms, 600)	69	0.9×10^3	n.d.	2.5	32	0.7	30	14	3	18
HZSM-5(ss, 400)	100	6.9×10^3	0.08	1.7	33	0.3	39	7	0.0	18
HZSM-5(ss, 450)	95	$>2.0 \times 10^4$	0.06	0.9	31	0.2	48	3	0.0	17
HZSM-5(ss, 500)	87	7.7×10^3	n.d.	2.6	29	0.4	48	5	2	13
HZSM-5(ss, 550)	49	1.9×10^3	0.04	0.9	30	0.2	52	0.9	5	11
HZSM-5(ss, 600)	12	7.6×10^2	0.01	2.8	41	0.7	47	0.0	0.0	8

^a Turnover number: number of moles of methanol converted into products different from dimethyl ether per BAS; the concentration of BAS is the value from pyridine IR after evacuation at 300 °C;

^b Determined after 34 h of reaction by TGA analysis.

dimethyl ether) per BAS. TON is determined until stable methanol conversion was obtained (detailed procedure outlined in Fig. S2). The values for HZSM-5 and HZSM-5(ms, 400) are almost similar (Table 5). The TON values decrease with increasing temperature of mild steaming and, accordingly, with increasing concentration of BAS. HZSM-5(ms, 600) deactivates almost instantaneously. The changes in catalytic performance are substantially different for the severely steamed zeolites. The methanol conversion after 1 h for HZSM-5(ss, 400) was 100%. The conversion after 1 h decreased significantly for the other severely steamed zeolites. The main selectivity differences with the mildly steamed zeolites is the higher combined ethylene and propylene selectivity, which increases from 72 to 88% with increasing steaming severity and lower propane selectivity. Importantly, the TON values are much higher for all severely steamed zeolites compared to the mildly steamed ones. For HZSM-5(ss, 450), it is more than an order of magnitude higher than for HZSM-5. Note that this zeolite exhibit a relatively high conversion after a reaction time of 34 h, so that its TON value represents a lower bound.

Several spent severely steamed zeolites were further analyzed for their coke content by TGA analysis. The coke content was typically lower than for the spent parent zeolite. The coke content decreased with increasing steaming temperature, which can be associated with the lower amount of methanol converted. The least active HZSM-5(ss, 550) and HZSM-5(ss, 600) produce very small amounts of coke. From the observation that the maximum weight loss during air calcination occurs at 560 °C, it can be concluded that the type of coke formed in all zeolites is similar and corresponds to polyaromatic species.

4. Discussion

The acidity of HZSM-5 zeolite can be varied by treatment in steam at elevated temperatures. The severity of the steam treatment was adjusted by varying the flow of water vapor and the temperature. The XRD and physisorption data indicate that the structure and porosity of HZSM-5 was not significantly affected by the hydrothermal treatment. The crystallinities of all zeolite samples remain higher than 90%. Severe steaming (high steam flow) resulted in slightly larger changes (lower crystallinity and cell volume) with a clear trend as a function of the treatment temperature than mild steaming (low steam flow). The contraction of the cell volume is due to the removal of Al from the zeolite lattice. This is consistent with the higher degree of dealumination for the severely steamed zeolites as follows from ^{27}Al NMR spectroscopy. The observation that the crystallinity remains high despite removal of Al has been explained by Ong et al. [31]. These authors discussed reorganization of defects sites by migration of silicic acid species. The micropore surface area and volume of steamed zeolites slightly decreased compared to the parent HZSM-5 zeolite. Despite this, textural characterization does not evidence the generation of significant mesoporosity during such steaming treatments.

^{27}Al NMR spectroscopy shows that steaming affected the Al speciation in the zeolites. Compared to the parent zeolite, the steamed zeolites contain more NMR-invisible and octahedral Al atoms. The degree of dealumination is, however, quite small for the mildly steamed zeolites. The octahedral Al atoms are highly dispersed and close to the framework, following from the observation that they revert to tetrahedral positions upon exposure to ammonia. The fraction of NMR-invisible Al atoms increased slightly with steaming temperature. It is well established that the second-order quadrupolar interactions of Al nuclei with local electric field gradients can broaden the ^{27}Al MAS NMR signal of species with lower or distorted coordination symmetries [43]. NMR-invisible Al atoms exist in a highly distorted tetrahedral

coordination, resulting in high quadrupolar coupling constants, which cause peak broadening outside detection in the 1D spectrum. These extra-framework Al atoms may be located at ion-exchange sites of the zeolite [31].

IR spectroscopy of adsorbed pyridine shows that the parent HZSM-5 zeolite predominantly contains BAS next to a small amount of LAS. Steaming at low temperatures ($T < 500$ °C) did not affect the acid site density. However, when steaming was carried out in the temperature range 500–600 °C, the BAS content increased. Concomitantly, the LAS concentration decreases slightly. These findings point to re-alumination of the framework. It has already been established earlier that Al atoms can insert in the framework of an already synthesized zeolite [44]. At relatively low temperatures ($T \approx 350$ °C), this is the result of reactions of Al^{3+} with internal hydroxyl nests, whereas at higher temperatures ($T > 500$ °C), direct substitution of Si^{4+} by Al^{3+} may also take place [45]. Therefore, it is assumed that extra-framework Al atoms are substituting Si framework atoms during mild steaming. Small amounts of water may promote the structural reorganization of the framework. In spite of being lower than for the parent zeolite, the cell volume of HZSM-5(ms, 550) is the highest among the mildly steamed zeolites, consistent with the proposal of Al insertion. A further indication is the higher intensity of the bands related to strong BAS in the IR spectra of adsorbed CO for HZSM-5(ms, 550) as compared to HZSM-5.

When HZSM-5 was steamed severely (high steam flow), a substantial portion of the framework aluminum was removed. This is evident from the higher fraction of Al^{VI} and distorted Al (distorted tetrahedral or penta-coordinated) atoms observed around 0 and 30 ppm, respectively, in the ^{27}Al NMR spectra. It is also found that a larger fraction of Al atoms becomes NMR-invisible. In contrast to the mildly steamed zeolites, ammonia treatment did not lead to significant changes in the Al speciation (cf. Fig. 2 and Table 2). From this, it follows that a larger part of the framework Al has segregated into an aluminum-rich phase as compared to the mildly steamed zeolites. Clearly, the tetrahedral peak in the 1D ^{27}Al NMR spectra of the severely steamed samples consists of two components, one around 56 ppm and another one around 53 ppm. The spectra in Fig. 1 show that the former band decreases stronger at intermediate steaming temperatures than the latter. This observation is in agreement with the results of Ong et al. [31]. The two resonances are due to isolated and grouped $\text{Si}(\text{OH})\text{Al}$ groups, respectively. Ong et al. found that steaming at 450 °C removed only the isolated Al atoms. The present data show that both types of Al atoms can be removed at higher steaming temperatures. Consistent with the trend of increasing framework Al removal, the pyridine IR results show a substantial decrease in Brønsted acidity with increasing severe-steaming temperature. Removal of framework Al already starts during steaming at 400 °C.

With respect to acid activity of these zeolites, it is useful to discuss first the propane conversion data (Table 4). The highest propane conversion rate was observed for the sample mildly steamed at 550 °C. The activity of HZSM-5(ms, 550) was significantly higher than that of the parent zeolite. The activity increase correlates well with the higher concentration of BAS as probed by IR spectroscopy of adsorbed pyridine. Niwa et al. have also found that treatment in ammonia/water at relatively low temperatures increases the protolytic cracking rate [32]. These authors ascribed the acidity increase to removal of Si from the framework, although no clear evidence was provided for this. Earlier, such enhancement of *n*-alkane cracking activity by dealumination of HZSM-5 has also been attributed to synergy between extra-framework Al and BAS [14]. Such an explanation does not appear to hold for the present set of mildly steamed ZSM-5 zeolites. For the severely steamed zeolites, the propane conversion rate strongly decreased with increasing steaming temperature. This trend is

consistent with the strong decrease in the concentration of BAS probed by pyridine and CO IR as well as of framework Al from NMR spectroscopy. Besides, Table 4 shows that differences in BAS content affect the protolytic cracking and dehydrogenation of propane in almost similar ways. In all of these cases, no significant contribution of extra-framework Al atoms on the rate of propane dehydrogenation can be derived from the catalytic activity data. Summarizing, a low steam flow results in very small changes to the Al distribution in the parent HZSM-5 zeolites. If at all, some framework defects heal, resulting in a greater number of Brønsted acid sites. A high steam flow results in severe dislodging of Al from the zeolite framework, resulting in significantly smaller numbers of Brønsted acid sites. At the employed conditions, the damage to the micropore structure of the zeolites is very limited.

The activity trends during methanol conversion with the steaming severity were different. All of the catalysts deactivated with reaction time. However, deactivation is only observed after a substantial reaction time, unless the total amount of BAS is low such as for the severely steamed ZSM-5 zeolites, resulting in partial methanol conversion. Textural characterization indicates that the various steaming procedures of the parent HZSM-5 zeolite did not generate noticeable mesoporosity, so that the trends are mainly the consequence of differences in the BAS content and, possibly, their location. The increased BAS content of the zeolites steamed under mild conditions with temperature resulted in more rapid deactivation. Consequently, the TON decreased with increasing BAS content for the mildly steamed zeolites (cf. Table 5). In line with this trend, a strong decrease in the BAS density for the severely steamed zeolites resulted in better utilization of the acid sites. The optimum is observed for HZSM-5(ss, 450) with nearly an order of magnitude higher TON than the parent zeolite. A further decrease in the concentration of BAS by more severe steaming resulted in lower initial methanol conversion and decreased TON. Fig. 5 shows the relation between TON and concentration of BAS as well as the TON based on the total amount of methanol converted ($\text{TON}_{\text{total}}$, taken into account also dimethylether). $\text{TON}_{\text{total}}$ increases strongly with decreasing BAS density. The difference between $\text{TON}_{\text{total}}$ and TON relates to formation of dimethyl ether. The total amount of dimethyl ether increases when the zeolite catalysts contain less BAS.

Currently, methanol conversion in zeolites is mainly discussed in terms of the hydrocarbon-pool mechanism involving methylated aromatic species [46], although for HZSM-5 alkene methylation has also been proposed for formation of higher hydrocarbons [47]. The hydrocarbon-pool species undergo methylation by methanol and/or dimethylether followed by elimination of light olefins. These olefins can be further converted via carbenium-ion chemistry into higher hydrocarbons and ultimately also into coke.

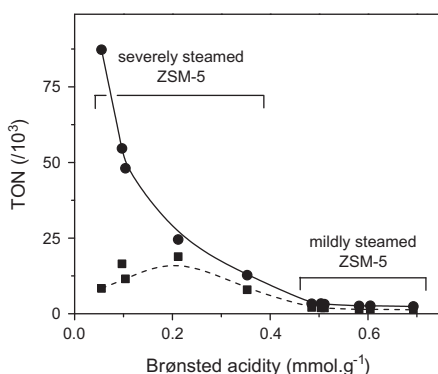


Fig. 5. (●) $\text{TON}_{\text{total}}$ based on total methanol converted and (■) TON based on methanol converted to products other than dimethyl ether.

The present data clearly show that a high concentration of BAS causes rapid deactivation due to the high rates of consecutive reactions of olefins, resulting in carbonaceous deposits (oligomers, aromatics). In such case, the total amount of methanol converted is low. The higher rate of coke formation at high BAS concentration is well known and has been suggested to relate to proximate BAS for multipoint adsorption [48]. Taulelle and colleagues recently showed the importance of proximate BAS for bimolecular hydride transfer reactions [49]. Although the authors of Ref. [47] contended that coke formation predominantly occurs on the external surface of HZSM-5, our correlation between TON and BAS concentration would appear to indicate the opposite, namely that coke forms throughout the ZSM-5 micropore space. This is further supported by recent UV-Vis and confocal fluorescence microscopy for large ZSM-5 crystals [50]. When the BAS content decreases, the rate of coke formation and thus catalyst deactivation becomes lower. This interpretation is in line with the decreasing amount of coke deposits for less acidic zeolites (cf. Table 5). Because of the low acidity, the reaction is largely limited to reacting methanol to dimethylether. Therefore, formation of products with carbon-carbon bonds is maximal at an intermediate BAS concentration. For the parent zeolite and the methanol conversion reaction conditions used in this study, this optimum is approximately 0.2 mmol g^{-1} .

It is worthwhile to discuss two possible alternative explanations for the lower rate of deactivation for less acidic zeolites, *i.e.*, (i) lower acidity of the protons remaining after severe steaming and (ii) preferential removal of Al at the outer zones of the zeolite crystals. The first hypothesis can be discarded, because the propane cracking activity data correlate well with the BAS content. This is expected, as it is well known that the acid sites in HZSM-5 exhibit similar acidity over a wide range of Si/Al ratios [1,51]. To probe whether severe steaming has preferentially removed strong BAS from the external zeolite surface, the IR spectroscopy data of adsorbed 2,4,6-trimethylpyridine are instructive. The results in Table 3 show that the amount of BAS accessible to this probe increased with steaming severity. This is most likely caused by structural damage at the external surface of the zeolite crystals. Ar physisorption apparently does not pick up such small changes in the porosity. Given these results, it can be concluded that differences in the activity of steamed ZSM-5 zeolites in the methanol conversion reaction depend predominantly on the total concentration of BAS.

5. Conclusion

The influence of mild ($8.2 \times 10^{-5} \text{ mol min}^{-1}$, 6 h) and severe ($3.3 \times 10^{-4} \text{ mol min}^{-1}$, 6 h) steaming at varying temperatures (400–600 °C) on the physicochemical properties of a HZSM-5 zeolite (Si/Al = 27) and its acid catalytic activity in monomolecular propane cracking and methanol conversion was investigated. Mild steaming does not result in removal of Al atoms from the framework. Instead, it was found that some extra-framework Al atoms present in the parent zeolite were inserted in the framework at defect sites, resulting in an increase in the BAS and higher propane conversion rates. Severe steaming results in a strong decrease in the framework Al content, agglomeration of the extra-framework Al atoms, and decreased Brønsted acidity as probed by IR spectroscopy of adsorbed pyridine and CO as well as catalytically by decreased propane conversion rates. The steaming procedures did not result in the formation of noticeable mesoporosity. IR spectroscopy of adsorbed 2,4,6-trimethylpyridine pointed to structural damage at the outer zones of the zeolite crystals, resulting in increased accessibility of a small part of the BAS.

For methanol conversion ($T = 350 \text{ °C}$), the catalytic performance is governed by the concentration of BAS. For zeolites with a high

BAS density (parent and mildly steamed zeolites), the rate of deactivation is high. The total amount of methanol converted per BAS is relatively low because of the high rate of consecutive reactions. These reactions involve the conversion the dehydration product of methanol, dimethyl ether, to products with carbon–carbon bonds and the formation of carbonaceous deposits, which deactivate the zeolite catalyst. Decreasing the acidity by severe steaming resulted in increased amounts of methanol converted per BAS because of a lower rate of coke formation. Because of this, the total amount of methanol converted per BAS increased strongly with decreasing BAS density. However, it also caused lower rates of conversion of the dimethyl ether intermediate to useful products. In terms of the total amount of methanol converted per BAS to useful products, mainly light olefins, the set of zeolites showed optimum performance at intermediate BAS density (HZSM-5 severely steamed at 450 °C with a BAS concentration of ~ 0.2 mmol g^{-1}).

Appendix A. Supplementary material

Supplementary data associated with this article can be found, in the online version, at <http://dx.doi.org/10.1016/j.jcat.2013.07.021>.

References

- [1] J. Cejka, A. Corma, S. Zones (Eds.), *Zeolites and Catalysis*, Wiley-VCH, Weinheim, 2010.
- [2] N.Y. Topsoe, F. Joensen, E.G. Derouane, *J. Catal.* 110 (1988) 404.
- [3] D.B. Lukyanov, *Zeolites* 11 (1991) 325.
- [4] D.B. Lukyanov, *Zeolites* 14 (1994) 233.
- [5] J. Datka, S. Marschmeyer, T. Neubauer, J. Meusinger, H. Papp, F.W. Schütze, I. Szpyt, *J. Phys. Chem.* 100 (1996) 14451.
- [6] A. Redondo, P.J. Hay, *J. Phys. Chem.* 97 (1993) 11754.
- [7] Y. Hong, J.J. Fripiat, *Microporous Mater.* 4 (1995) 323.
- [8] S. Kumar, A.K. Sinha, S.G. Hegde, S. Sivasanker, *J. Mol. Catal. A* 154 (2000) 115.
- [9] P.J. Kooyman, P. van der Waal, H. van Bekkum, *Zeolites* 18 (1997) 50.
- [10] G.W. Skeels, D.W. Breck, in: D.H. Olson, A. Bisio (Eds.), *Proceedings of 6th International Zeolite Conference*, Butterworths, Guildford, 1984.
- [11] L.J. Jin, H.Q. Hu, X.Y. Wang, C. Liu, *Ind. Eng. Chem. Res.* 45 (2006) 3531.
- [12] S. Han, D.S. Shihabi, C.D. Chang, *J. Catal.* 196 (2000) 375.
- [13] T. Masuda, Y. Fujikata, S.R. Mukai, K. Hashimoto, *Appl. Catal. A* 172 (1998) 73.
- [14] R.M. Lago, W.O. Haag, R.J. Mikowsky, D.H. Olson, S.D. Hellring, K.D. Schmitt, G.T. Kerr, in: Y. Murakami et al. (Eds.), *Proceedings of the 7th International Zeolite Conference*, Kondansha, Tokyo, 1986, p. 677.
- [15] R.A. Beyerlein, C. ChoiFeng, J.B. Hall, B.J. Huggins, G.J. Ray, *Top. Catal.* 4 (1997) 27.
- [16] M.A. Kuehne, H.H. Kung, J.T. Miller, *J. Catal.* 171 (1997) 293.
- [17] S.M. Campbell, D.M. Bibby, J.M. Coddington, R.F. Howe, R.H. Meinhold, *J. Catal.* 161 (1996) 338.
- [18] J. Datka, E. Tuznik, *J. Catal.* 102 (1986) 43.
- [19] A. Brunner, H. Ernst, D. Freude, M. Hunger, C.B. Krause, D. Prager, *Zeolite* 9 (1989) 101.
- [20] Y. Sendoda, Y. Ono, *Zeolite* 8 (1988) 101.
- [21] L. Yingcai, J.M.S. Yaojun, W. Tailiu, W. Liping, F. Lun, *J. Chem. Soc. Faraday Trans.* 92 (1996) 1647.
- [22] J.A. Martens, W. Souvrijns, W. van Rhijn, P.A. Jacobs, in: G. Ertl, H. Knözinger, J. Weitkamp (Eds.), *Handbook of Heterogeneous Catalysis*, vol. 1, Wiley-VCH, 1997, p. 324.
- [23] V.L.C. Gonçalves, R.C. Rodrigues, R. Lorençato, C.J.A. Mota, *J. Catal.* 248 (2007) 158.
- [24] J. Huang, Y. Jiang, R.V.R. Marthala, B. Thomas, E. Romanova, M. Hunger, *J. Phys. Chem. C* 112 (2008) 3811.
- [25] J. Jiao, J. Kanellopoulos, W. Wang, S.R. Sidarth, H. Foerster, D. Freude, M. Hunger, *Phys. Chem. Chem. Phys.* 7 (2005) 3221.
- [26] J. Jiao, S.S. Ray, W. Wang, J. Weitkamp, M. Hunger, *Z. Anorg. Allg. Chem.* 631 (2005) 484.
- [27] E.A. Pidko, E.J.M. Hensen, R.A. van Santen, *Proc. Roy. Soc. A* 468 (2012) 207020.
- [28] R. Carvajal, P.J. Chu, J.H. Lunsford, *J. Catal.* 125 (1990) 123.
- [29] J. Scherzer, T.E. White, R.A. Della Betta, E.G. Derouane, R.K.T. Baker (Eds.), *Catalytic Materials: Relationship Between Structure and Activity*, vol. 248, A.C.S. Symp. American Chemical Society, Washington, D.C., 1984, p. 157.
- [30] A. Maijanen, E.G. Derouane, J.B. Nagy, *Appl. Surf. Sci.* 75 (1994) 204.
- [31] L. Ong, M. Dömök, R. Olindo, A.C. van Veen, J.A. Lercher, *Microporous Mesoporous Mater.* 164 (2012) 9.
- [32] M. Niwa, S. Sota, N. Katada, *Catal. Today* 185 (2012) 17.
- [33] L.R. Aramburo, E. de Smit, B. Arstad, M.M. van Schooneveld, L. Sommer, A. Juhin, T. Yokosawa, H.W. Zandbergen, U. Olsbye, F.M.F. de Groot, B.M. Weckhuysen, *Angew. Chem., Int. Ed.* 51 (2012) 3616.
- [34] L.R. Aramburo, L. Karwacki, P. Cubillas, S. Asahina, D.A.M. de Winter, M.R. Drury, I.L.C. Buurmans, E. Stavitski, D. Mores, M. Daturi, P. Bazin, P. Dumas, F. Thibault-Starzyk, J.A. Post, M.W. Anderson, O. Terasaki, B.M. Weckhuysen, *Chem. Eur. J.* 17 (2011) 13773.
- [35] A.T. Aguayo, A.G. Gayubo, R. Vivanco, M. Olazar, J. Bilbao, *Appl. Catal. A. Gen.* 283 (2005) 197.
- [36] W. Dai, X. Wang, G. Wu, N. Guan, M. Hunger, L. Li, *ACS Catal.* 1 (2011) 292.
- [37] J. Datka, A.M. Tutek, J.H. Jehng, I.E. Wachs, *J. Catal.* 135 (1992) 186.
- [38] N.S. Nesterenko, F. Thibault-Starzyk, V. Montouillout, V.V. Yushchenko, C. Fernandez, J.-P. Gilson, F. Fajula, I.I. Ivanova, *Kin. Catal.* 47 (2006) 40.
- [39] E.J.M. Hensen, D.G. Poduval, D.A.J.M. Ligthart, J.A.R. van Veen, M.S. Rigutto, *J. Catal.* 269 (2010) 201.
- [40] J.A. van Bokhoven, A.M.J. van der Eerden, D.C. Koningsberger, *Stud. Surf. Sci. Catal.* 142 (2002) 1885.
- [41] E. Selli, L. Forni, *Microporous Mesoporous Mater.* 31 (1999) 129.
- [42] K. Chakarova, K. Hadjiivanov, *J. Phys. Chem. C* 115 (2011) 4806.
- [43] P.O. Fritz, J.H. Lunsford, *J. Catal.* 118 (1985) 85.
- [44] M.W. Anderson, J. Klinowski, L. Xinsheng, *J. Chem. Soc. Chem. Commun.* (1984) 1596.
- [45] T. Yashima, K. Yamagishi, S. Namba, S. Nakata, S. Asaoka, *Stud. Surf. Sci. Catal.* 37 (1987) 175.
- [46] I.M. Dahl, S. Kolboe, *J. Catal.* 149 (1994) 458.
- [47] M. Björgen, S. Svelle, F. Joensen, J. Nerlov, S. Kolboe, F. Bonino, L. Palumbo, S. Bordiga, U. Olsbye, *J. Catal.* 249 (2007) 195.
- [48] D.M. Bibby, R.F. Howe, G.D. McLellan, *Appl. Catal. A* 93 (1992) 1.
- [49] S. Borghèse, M. Haouas, J. Sommer, F. Taulelle, *J. Catal.* 305 (2013) 130.
- [50] D. Mores, J. Kornatowski, U. Olsbye, B.M. Weckhuysen, *Chem. Eur. J.* 17 (2011) 2874.
- [51] W.O. Haag, R.M. Lago, P.B. Weisz, *Nature* 309 (1984) 589.